Imaging the Plumbing System of the Asymmetric Vavilov Spreading Ridge (Tyrrhenian Sea Back-Arc Basin) From Combined Bathymetry and Magnetic Data

L. Cocchi[1] [ID]**, F. Muccini[1]** [ID]**, C. Palmiotto[2]** [ID]**, and G. Ventura[1,3]** [ID]

[1]Istituto Nazionale di Geofisica e Vulcanologia, Rome, Italy, [2]Consiglio Nazionale delle Ricerche, Istituto di Scienze Marine, Bologna, Italy, [3]Consiglio Nazionale delle Ricerche, Istituto Per Lo Studio Degli Impatti Antropici E Sostenibilità In Ambiente Marino, Torretta Granitola (TP), Italy

Abstract Back-arc basins (BABs) are associated with plate margins where crustal shortening, seafloor spreading, and volcanism coexist. The Vavilov basin (Tyrrhenian Sea) is a Pliocene BAB associated with the Apennine-Tyrrhenian Sea subduction system and characterized by mantle exhumation. The NNE-SSW elongated Vavilov seamount represents the easternmost and younger spreading ridge of the Vavilov basin. Here we present results of a morphological and magnetic study of the Vavilov seamount. Our results show that the seamount represents the last stage of the eastward asymmetric opening of the BAB. Its plumbing system consists of a dike swarm emplaced during the reversed Matuyama epoch and a younger shallow reservoir feeding the central and eastern sectors during the normal Brunhes epoch. This evolution is associated with the progressive loading of the edifice due to lava flow emplacement. The asymmetry of the seamount mirrors the asymmetric opening of the Vavilov back-arc basin.

Plain Language Summary Stretching of the crust, seafloor spreading, and volcanism occur in the overriding plate above roll-backing slabs in subduction settings. The Vavilov basin (Tyrrhenian Sea) is a back-arc associated with the eastward retreating of the Apennine-Tyrrhenian Sea subduction system. The NNE-SSW elongated Vavilov submarine volcano represents the easternmost and younger spreading center of this back-arc basin. Combined morphological and magnetic studies of the Vavilov seamount show that the plumbing system of the seamount consists of an early sheet-like intrusion system and a younger, central reservoir feeding the magmatism of the central and eastern sectors of the spreading ridge. This evolution is associated with the progressive growth of the edifice due to lava flow emplacement. The morphological and magnetic asymmetry of the seamount is due to the eastward, asymmetric opening of the Vavilov back-arc basin.

1. Introduction

Back-arc basins (BABs) reflect extensional processes and volcanism at convergent plate margins where subduction occurs (Artemieva, 2023; Karig, 1971; Schliffke et al., 2022; Stern, 2002). BABs formation is characterized by an early crustal stretching phase followed by seafloor spreading and volcanism associated with active uplift (Dunn & Martinez, 2011) or passive exhumation (Prada et al., 2016) of the mantle. The spreading processes in BABs are strictly associated to the movements of the slab (e.g., roll-back) and to the mantle dynamics in the overriding plate (Holt & Royden, 2020; Li et al., 2018; Sdrolias & Müller, 2006; Wei & Wiens, 2020). Because of the close spatial association of BABs and subduction zones, the composition of the BABs erupted magmas generally involves both mantle and slab components (Pearce & Stern, 2006). While the broad morphology and inner structure of major BABs with seafloor spreading is relatively known (Anderson et al., 2017; Caratori Tontini et al., 2019; Palmiotto, Braga, et al., 2022), that of the spreading ridges associated with smaller scale, localized BABs related to the passive exhumation of the mantle is less known and still enigmatic. Open questions include the relation between fissural and central-type volcanism and the geometry of the plumbing system. Here we present a joint magnetic and morphological analysis of the 2.6–2.4 Ma to 0.37–0.09 Ma old Vavilov volcano (VAV) (central Tyrrhenian Sea) (Kastens et al., 1988; Savelli & Ligi, 2017). VAV represents the spreading ridge of the 3,600 m deep, ∼7 Ma old Vavilov back-arc basin (VBAB). Our aim is to investigate the VAV plumbing system and its relations with the surface volcanic and tectonic structures. Results show that the spreading ridge of small BABs may be characterized by a polyphase evolution from fissural to central-type volcanism and by a multi-level plumbing system. In addition, we provide evidence for the migration of activity related to asymmet-

ric spreading processes, a feature observed in many BABs including Tonga, Ryukyu, Kuril, and New Hebrides (Schellart et al., 2003). The geodynamic implications for the formation of the VBAB and other BABs are also discussed.

2. Geodynamic and Volcanological Setting

VBAB is located in the central Tyrrhenian Sea and it is associated to the eastward migration of the Apennine chain in response to the roll-back process of the Adria slab (Figure 1a; e.g., Doglioni, 1991; Doglioni et al., 1999, 2004; Malinverno & Ryan, 1986). The basin shows a roughly triangular shape with major escarpments (i.e., Selli Line; Figure 1a) marking the boundaries with the continental margins (Cornaglia Terrace in Figure 1a; De Marchi Smt and Flavio Gioia Smt in Figure 1b). West of VAV, the basin is characterized by a set of N-S oriented ridges as expression of injection of basalts during (or post) mantle exhumation (i.e., Gortani ridge; Oceanic Drilling Program (ODP) Leg 107, sites 655a/b, Kastens et al., 1990; Figure 1b).

The emplacement of new oceanic crust in the VBAB has been questioned because MOR-like basalts have been sampled only on the VAV (Kastens et al., 1988; Mascle & Rehault, 1990; Sartori et al., 2004; Scrocca et al., 2012). Samples from drilling the VBAB abyssal plain (ODP 651; Kastens et al., 1990) indicate the presence of serpentinized mantle peridotites beneath a layer of calc-alkaline basalts (2.6 Ma; Bonatti et al., 1990; Sartori et al., 2004). Site 373 of Deep Sea Drilling Project (DSDP) recorded a sequence of basalts and breccia dated >4.1 Ma (Hsu et al., 1978). According to Milia et al. (2017), volcanic rocks at the site 373 mark the VBAB pre-rifting stage. Shear-wave velocity models of Prada et al. (2016), Manu-Marfo et al. (2019) and Magrini et al. (2022) and seismostratigraphic data of Milia et al. (2017) support the presence of exhumed mantle. Loreto et al. (2021) propose that the VBAB was affected by a Pliocenic rifting phase dominated by a mantle exhumation and by a later injection of MOR–like basalts. VAV is a NNE-SSW elongated, 35 km long and 16 km wide volcanic complex rising from the VBAB abyssal plain at 3,600 m below sea level (b.s.l., hereafter) to 795 m b.s.l. VAV consists of a sequence of lava flows and basaltic pillows having a MOR-like affinity (low Heavy-Rare-Earth Elements-enriched tholeiites, Robin et al., 1987); alkali basalts possibly related to a subduction component have been also found (Robin et al., 1987).

VAV consists of three main volcanic units: pillow lavas (beneath 1,500 m depth), radial lava flows (from 1,500 m to 1,000 m), scoriaceous lava flows (from 1,000 m to the summit; Robin et al., 1987). These authors recognize two principal eruptive centers located above 1,500 m b.s.l. and minor centers along the main ridge aligned NNE-SSW. Submarine lavas sampled at the base of the volcano were dated at about 2.6–2.4 Ma (Upper Pliocene; Kastens et al., 1988; Sartori et al., 2004; Savelli, 2002). K-Ar dating of pillows sampled along the eastern flanks at depth of 1,000 m show Pleistocene ages of 0.37 and 0.09 Ma (Robin et al., 1987) belonging into the normal Brunhes geomagnetic chron (C1n, <0.78 Ma; Cande & Kent, 1995). The shallower portion of VAV shows a general positive magnetic anomaly pattern consistent with the normal magnetic polarity (Faggioni et al., 1995). The base of the VAV is asymmetrical in E-W direction since the western side of the basin is about 200 m shallower than the eastern side. The western sector of VAV shows a steep flank with a smooth morphology suggesting the possibility of a flank collapse of the volcano (Gallotti et al., 2023).

3. Data and Methods

3.1. Bathymetric Data

High resolution bathymetric data of VBAB were acquired during MAVA 11 oceanographic cruise on board of Nave Magnaghi (Italian Navy; Muccini et al., 2016). A SeaBeam 1050 multibeam system operating at 70 kHz frequency, featured by 126 beams and resolution of $1.5° \times 1.5°$ was used to acquire the VAV bathymetry and part of the abyssal plain. The multibeam survey covered an area of about 1,800 km². Geo-referencing of multibeam data was ensured with a differential GPS Trimble Pathfinder XRS-PRO.

Raw bathymetric data were processed using the software Caris Hips and Sips 8.1 computing an interpolated surface with a cell size resolution of 25 m. High resolution bathymetry of VAV has been integrated with a 200 m gridded data from EMODnet data set (EMODnet Bathymetry Consortium, 2020) obtaining an overview of the VBAB morphology (Figure 1b). The morphometric and geomorphological analysis of VAV has been performed according to Gallotti et al. (2023) and the results are reported in Figure 2.
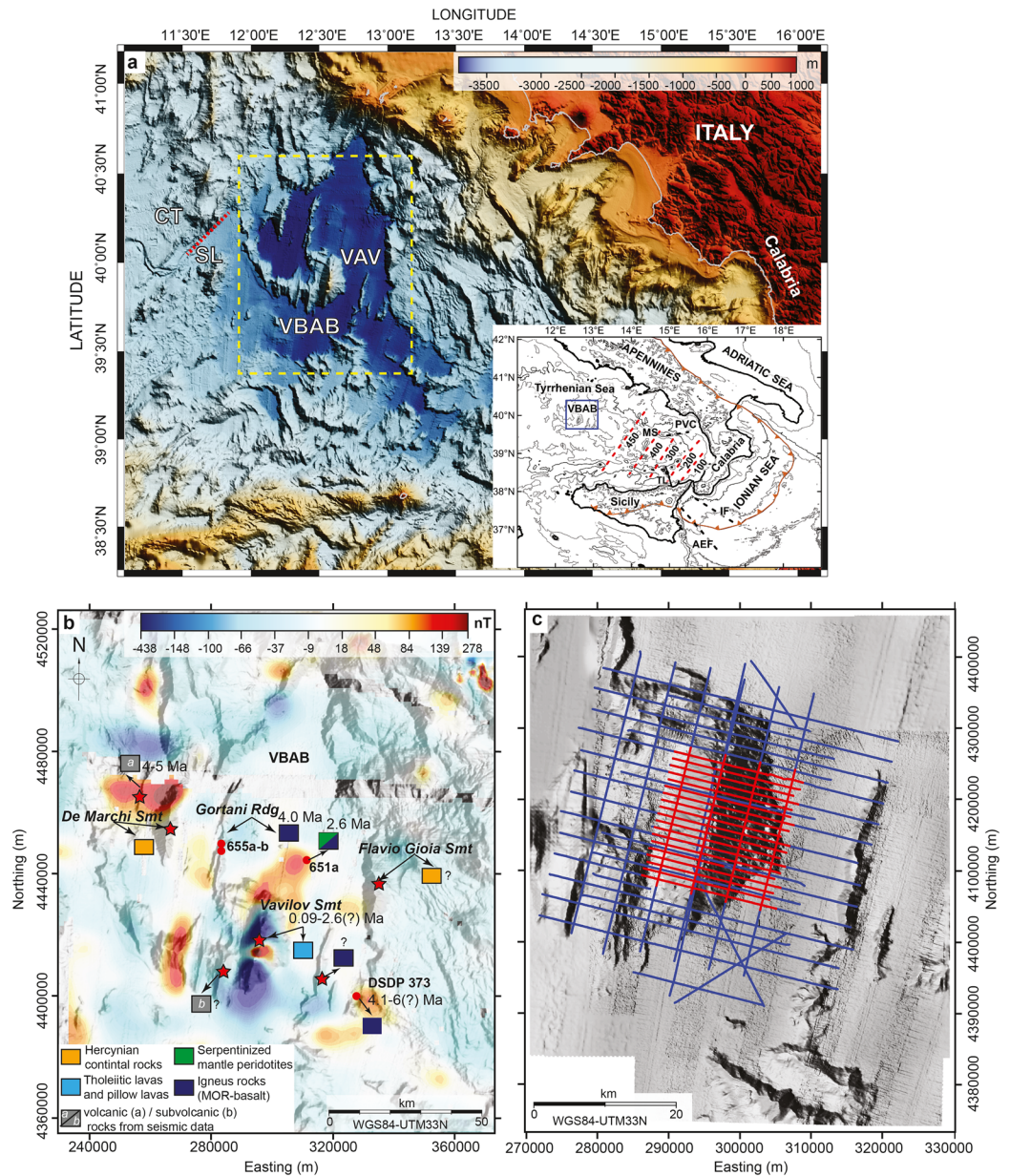
Figure 1. (a) Bathymetry map of the central-southern Tyrrhenian Sea showing major features discussed in the text. From west to east: Cornaglia Terrace (CT), Selli Line (SL), Vavilov Basin (VBAB), Vavilov seamount (VAV). Dashed yellow box identifies the study area. The inset represents the geodynamic sketch of southern Tyrrhenian Sea: Marsili Seamount (MS), Tindari Letojanni (TL); Palinuro volcanic complex (PVC; Cocchi et al., 2017); Ionian fault (IF), Alfeo Etna fault (AEF); red dashed lines mark the depth of Ionian subducted slab (Magrini et al., 2022; Polonia et al., 2017). (b) Regional magnetic anomaly field draped over bathymetry of VBAB (linepath in Figure S1 in Supporting Information S1). Red starts identify main morphologic structures of VBAB (data from Sartori et al., 2004); red dots indicate the position of the sites of seafloor drilling (Hsu et al., 1978; Kastens et al., 1990). (c) Morphology of VAV with the layout of magnetic surveys: blue lines were designed for investigating the edifice and surrounding basin, the red lines for investigating the volcanic crest.

3.2. Magnetic Data Acquisition and Modeling

Shipborne magnetic data of VAV were also collected during the MAVA11 cruise by using a SeaSpy Marine Magnetics magnetometer towed 180 m astern the ship. Positioning of the tow fish was estimated by applying a synchronous GPS layback correction. We conducted the geophysical investigation in two distinct surveys: (a) a larger one covering the entire VAV edifice and partly also its basin using a set of lines spaced 1,500 m (blue lines
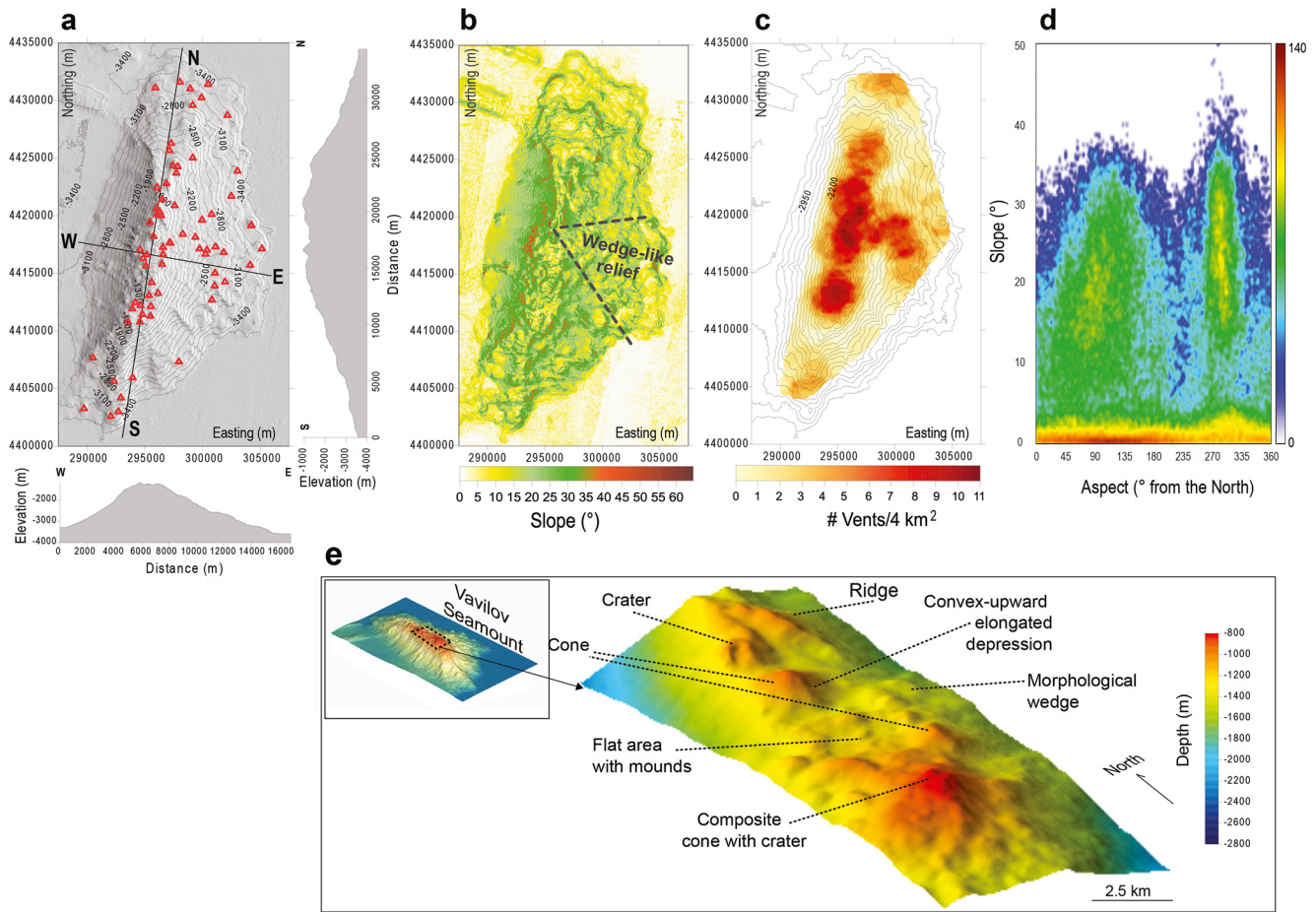
Figure 2. (a) Shaded relief map of VAV with superimposed 100 m spaced isobaths and E-W and N-S morphological profiles crossing the seamount. The red triangles show the location of volcanic vents (data from Gallotti et al., 2023). (b) Slope map of the VAV. The wedge-like relief discussed in the text is bounded by dashed lines. (c) Spatial density of the VAV volcanic vents reported in panel (a). (d) Aspect versus slope density plot of VAV obtained from the bathymetry data reported in panel (a). (e) 3D view of the VAV summit sector with interpretation of the main morphological structures.

in Figure 1c); (b) a second high resolution survey focused on VAV carried out using a set of lines spaced about 1,000 m (red lines in Figure 1c).

The two data sets were merged and processed removing spikes and heading effects (see methods in Cocchi et al., 2016). The magnetic anomaly field (Figure 3a) was calculated by subtracting the International Geomagnetic Reference Field model (IGRF; Alken et al., 2021) from the total magnetic field. Cross-over errors were estimated and reduced applying a statistical leveling technique. Reduced To the Pole (RTP, Baranov, 1957) anomaly data of VAV (Figure 3b) were computed using the local values of inclination (55.8°) and declination (2.3°) of magnetic vector derived from the IGRF model. Finally, magnetic data of VAV have been integrated into the regional magnetic data set of the VBAB collected by National Research Council (Bortoluzzi et al., 1999; Palmiotto, Braga, et al., 2022) (Figure 1b and Figure S1 in Supporting Information S1).

We inverted the magnetic data to reconstruct the inner structure of the VAV. The inversion focused on the central–summit portion of VAV being the area covered by the highest resolution data and where a set of alternating positive-negative magnetic polarities is observed (Figure 3b).

The inversion was constrained using a voxel mesh having the seafloor bathymetry as a top layer and a flat bottom layer placed at 6 km of depth. We selected the vertical extension of the mesh considering that: (a) the VBAB shows a shallow Moho discontinuity (≤10 km, Sartori et al., 2004) and (b) the target of the inversion is to reconstruct the shallow VAV plumbing system. The mesh consists of $239 \times 238 \times 85$ prismatic cells (cell-width of 100 m, 100 and 50 m, in X, Y and Z direction, respectively). The mathematical algorithm combines a Cartesian
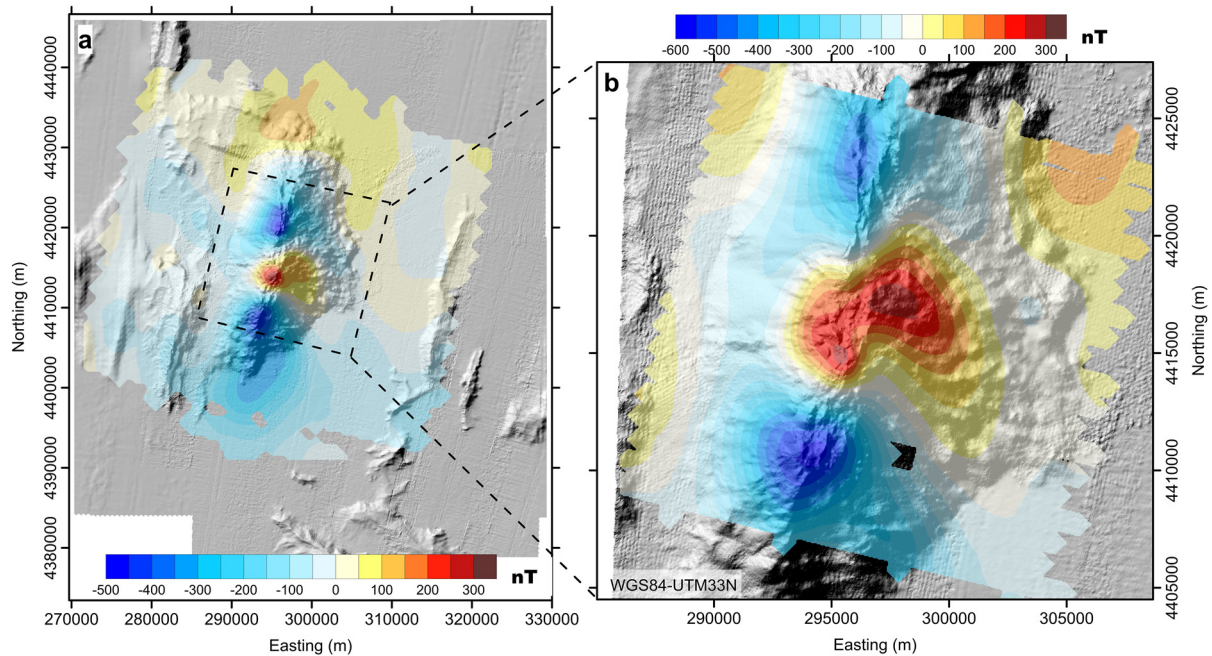
Figure 3. (a) Magnetic anomaly map of VAV and part of its basin superimposed on bathymetry. (b) High resolution reduced to the pole magnetic anomaly draped over 25 m grid cell size bathymetry of the summit crest.

cut cell approach (Ellis & MacLeod, 2013; Ingram et al., 2003) and an iterative reweighting inversion focusing (VOXI™) method in order to model sharp contacts.

Considering the lack of data about the remnant magnetic component, the inversion algorithm was parameterized by considering just the values of intensity and direction of the induced geomagnetic field. The positivity of the solutions was not forced because the data show multiple magnetic polarities.

4. Results

4.1. Morphology of the Vavilov Seamount

VAV is a NNE-SSW elongated volcanic complex with a summit, central ridge (Figures 2a–2e). This ridge preserves morphologies possibly related to volcanic landforms including cones, craters, rectilinear ridges (dikes), and morphologies related to gravity processes, that is, convex-upward elongated depressions that could be related to sliding (Figure 2e). A flat area with mounds has also been recognized (Figure 2e) possibly reflecting the surface expression of hydrothermal processes (Ventura et al., 2013).

The major, summit central VAV ridge separates in two slightly diverging ridges moving toward the northern and southern tip of VAV (Figure 2b), a feature observed in many fissural volcanoes and reflecting the control of the topographic load on dike propagation (Tibaldi, 2015). The smaller, western ridges departing from the central one delimit the western flank of the edifice and connect morphologically to the WNW-ESE elongated ridges of the VBAB abyssal plane (Figure 1b). The summit central ridge separates the two main VAV flanks. These flanks show different slope, aspect, and width values (Figure 2e). The western flank shows slopes concentrated between 12° and 32° and aspect between 270°N and 310°N. The eastern flank has slopes mainly between 8° and 28° with aspect between 40°N and 140°N. In addition, the western flank shows a relatively smooth surface and a width of about 5 km. The eastern flank exhibits a hummocky-like surface and a width of 9 km (Figure 2b). Small-scale volcanic cones concentrate on the central ridge and on the central sector of the eastern flank between the top of VAV and the eastern abyssal plain (Figures 2a and 2c). The occurrence of these cones explains the irregular morphology of this flank. These cones and their products (i.e., pillow lavas; Robin et al., 1987) create a larger scale, topographically elevated, wedge-like morphology whose apex coincides with the VAV summit and the base spreads over the eastern VBAB abyssal plain (Figures 2a and 2c). The morphological difference between the two

flanks results from an asymmetric growth of the volcano, although a contribution of past flank collapses can not be excluded (Gallotti et al., 2023).

4.2. Magnetic Pattern of Vavilov Seamount

VAV shows a negative magnetic anomaly pattern featured by high intensity minima (about −300 nT) located at its northern and southern tips (Figure 3a). The negative pattern is well confined to the northern and southern sectors of the edifice suggesting that the bulk of the volcano is mainly characterized by a natural remanent magnetization with reverse polarity. A local high intensity, positive magnetic anomaly (>200 nT) overlaps the central portion of VAV and part of the eastern flank (Figure 3b), which shows a dense distribution of volcanic vents (Figures 2b and 2c). The presence of an isolated positive magnetic body within a broad negative background suggests a time-scale evolution of the VAV activity during a reverse-to-normal polarity of the Earth's Magnetic field.

4.3. Large-Scale Magnetic Pattern and Age of the VBAB

The distribution of the VBAB magnetic anomaly field reflects its peculiar geodynamic evolution with a set of negative and positive N-S magnetic lineaments distributed at the western side of De Marchi seamount and in proximity of the Gortani ridge (Figure 1b). The variation in magnetic polarities suggests a temporal evolution of the emplacement of the N-S trending ridges. The Gortani ridge seems associated with negative anomalies reflecting its emplacement during the reversed late Gilbert epoch (C2Ar, 4.18–3.58 Ma), as also confirmed by the dating of rock samples (ODP 107 sites 655 a/b). Other minor ridges placed at west of Gortani and De Marchi are supposed to be emplaced during pre-Gilbert normal subcrones (supposed C3n, >4.18 Ma) considering polyphasic basaltic injections. This activity becomes younger moving from the western to eastern side of the basin testifying the VBAB asymmetric rifting (Milia et al., 2017). The VAV eastern sector shows a slight negative magnetic pattern (−100 to 20 nT), without evidence of N-S oriented magnetic anomalies as observed at the opposite side.

5. Discussion

5.1. Geometry of the VAV Plumbing System

A 3D inversion of magnetic data was performed in order to obtain information on the VAV shallow plumbing system (Figure 4). At the northern and southern VAV edges, two major NNE-SSW elongated bodies occur with high negative signature of −0.15 SI. The southern body has an inclined sheet-like geometry while the northern one shows a shape consistent with that of a vertical dike (Figure 4). Less extended, ellipsoidal bodies with a negative signature and a sill-like shape also occur at depths between 3 and 4 km. Below the VAV central sector we recognize a positive (max 0.17 SI), flower-like magnetic body located within the edifice and extending in depth from near the surface to 4.5 km b.s.l (Figure 4a). This body mirrors the shape of the intrusive, sill-like to flower-type bodies observed in central volcanoes (Tibaldi, 2015; Tibaldi & Pasquarè, 2008). A positive magnetic, NW-SE elongated apophysis departs from the VAV major, central flower-like structure extending 2–3 km in depth below the eastern sector.

We interpret the negative bodies as a major dike system formed during the pre-Olduvay Matuyama epoch (C2r, 2.581–1.950 Ma) and feeding the early activity of VAV (2.6–2.4 Ma, Robin et al., 1987; Savelli & Ligi, 2017). The surface expression of this system is represented by the NNE-SSW aligned cones located on the summit ridge. The positive, flower-like body located in the central sector of the volcano could represent a shallow reservoir emplaced during the Brunhes chron (C1n, <0.78 Ma) after the early, fissural phase. The positive, NW-SE elongated apophysis departing from the main positive body southeastward may represent a lateral intrusion. According to Clague et al. (2011) and Klügel et al. (2015), lateral intrusions are favored by an increase of the lithospheric stress related to the progressive edifice loading due to growth of the volcano. The transition from a fissural to central-type activity at VAV may be explained in light of experimental (Muller et al., 2001) and numerical (Pinel et al., 2017) models, which show that the increase of loading induced by a growing topography associated to the lava flow emplacement favor dyke-like conduits to converge in a single zone located below the volcano thus allowing the formation of shallow reservoirs.

Considering the results of the inverse model (Figure 4), we estimate that the volume of the central magnetic positive body is 263.94 km^3 while the whole VAV edifice has a total volume of about 1,048.23 km^3 (see Table S1
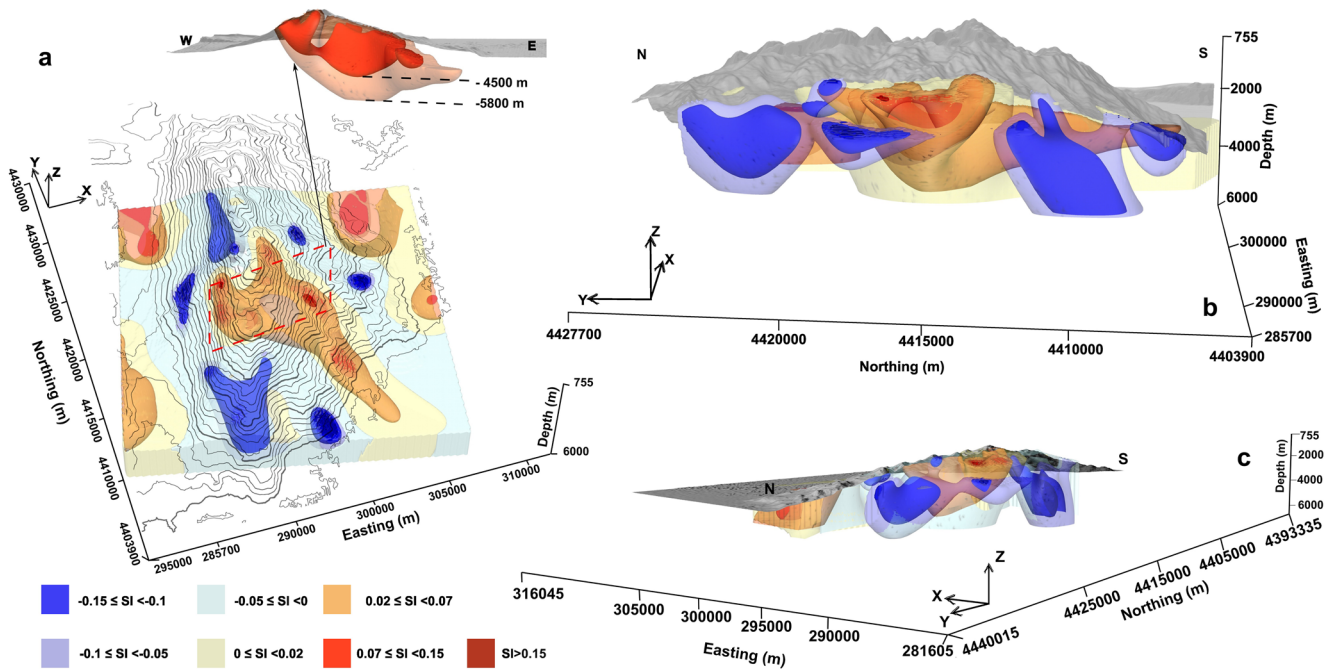
Figure 4. 3D inverse model of magnetic anomaly data of the VAV (Figure 3b). The panel sequence shows oblique perspectives from the plain view (a), west (b), and northwest (c). The bathymetric surface is also included in order to provide context of the main morphologic features of VAV.

in Supporting Information S1). Assuming that this body represents the crystallized magma reservoir emplaced between 0.37 and 0.09 Ma (from K-Ar dating of summit lavas; Robin et al., 1987), we estimate a minimum magma accumulation rate of 0.942×10^{-3} km^3 y^{-1}. This value is of the same order of magnitude of that estimated for intrusions with a prolonged recharge (10^{-3} km^3 y^{-1}; Menand et al., 2015). We deduce that the recent VAV eruptions mainly occurred shortly after single intrusive events because for smaller intrusion rates, the magma cools rapidly and its viscosity increases to values not allowing the ascent to the surface (Menand et al., 2015).

5.2. Geodynamic Significance of the VAV Volcanism in the General Evolution of the VBAB

The lack of a clear symmetry of the magnetic strips of VBAB as well as the occurrence of younger rocks on the eastern side of the BAB suggest that the N-S ridge structures of VBAB represent basaltic injections occurring along dikes formed in discrete time phases rather than associated with an active seafloor spreading as observed in other BABs (i.e., Marsili basin and North Lau Basin; Cocchi et al., 2009; Palmiotto, Ficini, et al., 2022). This agrees with more general geodynamic models suggesting that VBAB is not a classical, symmetric BAB but a basin dominated by mantle-exhumation processes related to the eastward migration of the subducting slab (Magrini et al., 2022; Manu-Marfo et al., 2019; Milia et al., 2017; Prada et al., 2016). This mechanism of formation of VBAB explains its rejuvenation moving from west to east, that is, from the ridge at west of De Marchi Smt to the Gordani ridge and VAV (Figure 1b). In this framework, these three main N-S elongated ridges represent fissural MOR-basalts whose activity ends when the deformation (extension) progressively migrated eastward.

The VBAB asymmetry resembles that of other BABs, that is, New Hebrides, East Scotia Sea, where it is explained by different mechanisms including migration of the ridge crest over the sub-asthenospheric mantle (Barker & Hill, 1980), asymmetric slab retreat due to irregular slab geometries, occurrence of Subduction-Transform Edge Propagators faults (STEP, Ha et al., 2023; Schellart et al., 2003). At VBAB, evidence of (a) possible thermal effects due to a sub-asthenospheric mantle, (b) sudden changes in slab geometry or STEP faults are lacking (Faccenna et al., 2001). This corroborates our conclusion that the VBAB asymmetry is related to the eastward roll-back of the slab below Apennines (Doglioni, 1991).

VAV is the largest of VBAB seamounts and may be interpreted as an inflated ridge formed during the last phase of aperture of the basin. This is confirmed by the presence of a thin layer of basalts dated 2.6 Ma overriding the mantle serpentinites (ODP 651, Bonatti et al., 1990).

The pattern of the VAV magnetic anomalies (Figure 3) clearly shows that while the negative pattern follows the large-scale morphology of the volcanic edifice, the positive magnetic anomaly overlaps the wedge-like morphologic structure including the vents located on the top and eastern flank of the volcano (Figure 2). We conclude that while the fissural activity of VAV developed mainly during a reversed Matuyama chron (C2r), the more recent volcanism of the central, apical sector and eastern flank occurred during the Brunhes chron (C1n). This interpretation agrees with the few available geochronological data on the VAV lavas sampled on the top of the volcano (0.37–0.09 Ma; Robin et al., 1987). This chronological evolution of volcanism could, at least in part, explain the morphological asymmetry of VAV. The occurrence of the more recent vents on the eastern flank and the associated products are responsible for the formation of the above mentioned wedge-like morphological relief and of the larger width of the eastern flank with respect to that of the western one. Such eastward and more recent concentration of the volcanism on the eastern VAV can be associated to the larger scale processes occurring in VBAB, whose evolution is controlled by an asymmetric, eastward opening of the basin, as previously reported. Therefore, the more recent activity of the VAV represents the last manifestation of volcanic activity within VBAB, possibly developed during the last phase of opening and/or at the end of the back-arc extension processes.

6. Conclusions

The results of our study may be summarized in the following main points:

1. Vavilov volcano represents the last manifestation of a series of basaltic injections in the homonymous basin, whose formation reflects prevailing mantle exhumation processes.
2. The early Vavilov activity developed along NNE-SSW dikes defined on the surface by aligned cones mainly emplaced during the reverse geomagnetic chron (C2r, 2.581–1.950 Ma). The more recent volcanism developed at the top of the edifice and on its eastern flank during the last normal geomagnetic chron (Brunhes, C1n, <0.78 Ma).
3. The morphological asymmetry of Vavilov volcano reflects the migration of activity from west to east with decreasing time and associated with the eastward, asymmetric opening of the basin.
4. The Vavilov shallow plumbing system consists of (a) an early dike sheet elongated NNE-SSW feeding the fissural activity of the summit ridge, and (b) a younger central reservoir located below the top of the volcano feeding the summit central vents. A NW-SE apophysis departing southeastward from the central reservoir possibly feeds part of the cones located on the Vavilov eastern flank.

Further geophysical and petrological studies on the other basaltic ridges of Vavilov basin should be carried out to better understand the mechanisms of fissural spreading in asymmetric BABs and define a general model of the deeper portion of the plumbing system of back-arc spreading centers.

Data Availability Statement

MAVA 11 datasets are accessible from the Figshare repository (Cocchi, 2023). Bathymetry data of Tyrrhenian Sea region are downloadable at EMODnet Bathymetry Consortium (2020). Some figures were prepared with Generic Mapping Tools software (GMT; Wessel & Smith, 1998).

References

Alken, P., Thébault, E., Beggan, C. D., Amit, H., Aubert, J., Baerenzung, J., et al. (2021). International geomagnetic reference field: The thirteenth generation. *Earth, Planets and Space*, *73*(1), 49. https://doi.org/10.1186/s40623-020-01288-x

Anderson, M. O., Chadwick, W. W., Hannington, M. D., Merle, S. G., Resing, J. A., Baker, E. T., et al. (2017). Geological interpretation of volcanism and segmentation of the Mariana back-arc spreading center between 12.7°N and 18.3°N. *Geochemistry, Geophysics, Geosystems*, *18*(6), 2240–2274. https://doi.org/10.1002/2017GC006813

Artemieva, I. M. (2023). Back-arc basins: A global view from geophysical synthesis and analysis. *Earth-Science Reviews*, *236*, 104242. https://doi.org/10.1016/j.earscirev.2022.104242

Baranov, V. (1957). A new method for interpretation of aeromagnetic maps: Pseudo-gravimetric anomalies. *Geophysics*, *22*(2), 359–382. https://doi.org/10.1190/1.1438369

Barker, P. F., & Hill, I. A. (1980). Asymmetric spreading in back-arc basins. *Nature*, *285*(5767), 652–654. https://doi.org/10.1038/285652a0

Bonatti, E., Seyler, M., Channell, J., Girardeau, J., & Mascle, G. (1990). Peridotites drilled from the Tyrrhenian Sea, ODP LEG 107. *Proceedings of the Ocean Drilling Program, Scientific Results*, *107*, 37–47. https://doi.org/10.2973/odp.proc.sr.107.141.1990

Bortoluzzi, G., Carrara, G., Fabretti, P., Gamberi, F., Marani, M., Penitenti, D., et al. (1999). *Swath bathymetry and geophysical survey of the Tyrrhenian Sea. Report on bathymetric, magnetic and gravimetric investigations during cruises TIR96 and TIR99*. CRUISE REPORTS/Tir96, 99.

Cande, S. C., & Kent, D. V. (1995). Revised calibration of the geomagnetic polarity timescale for the late Cretaceous and Cenozoic. *Journal of Geophysical Research*, *100*(B4), 6093–6095. https://doi.org/10.1029/94JB03098

Caratori Tontini, F., Bassett, D., De Ronde, C. E. J., Timm, C., & Wysoczanski, R. (2019). Early evolution of a young back-arc basin in the Havre Trough. *Nature Geoscience*, *12*(10), 856–862. https://doi.org/10.1038/s41561-019-0439-y

Clague, D. A., Paduan, J. B., Caress, D. W., Thomas, H., Chadwick, W. W., & Merle, S. G. (2011). Volcanic morphology of West Mata Volcano, NE Lau Basin, based on high-resolution bathymetry and depth changes. *Geochemistry, Geophysics, Geosystems*, *12*(11). https://doi.org/10.1029/2011GC003791

Cocchi, L. (2023). MAVA11 magnetic dataset of Vavilov volcano [Dataset]. Figshare. https://doi.org/10.6084/m9.figshare.23579196.v2

Cocchi, L., Caratori Tontini, F., Muccini, F., Marani, M. P., Bortoluzzi, G., & Carmisciano, C. (2009). Chronology of the transition from a spreading ridge to an accretional seamount in the Marsili backarc basin (Tyrrhenian Sea). *Terra Nova*, *21*(5), 369–374. https://doi.org/10.1111/j.1365-3121.2009.00891.x

Cocchi, L., Masetti, G., Muccini, F., & Carmisciano, C. (2016). Geophysical mapping of Vercelli Seamount: Implications for Miocene evolution of the Tyrrhenian back arc basin. *Geoscience Frontiers*, *7*(5), 835–849. https://doi.org/10.1016/j.gsf.2015.06.006

Cocchi, L., Passaro, S., Tontini, F. C., & Ventura, G. (2017). Volcanism in slab tear faults is larger than in island-arcs and back-arcs. *Nature Communications*, *8*(1), 1451. https://doi.org/10.1038/s41467-017-01626-w

Doglioni, C. (1991). A proposal for the kinematic modelling of W-dipping subductions - Possible applications to the Tyrrhenian-Apennines system. *Terra Nova*, *3*(4), 423–434. https://doi.org/10.1111/j.1365-3121.1991.tb00172.x

Doglioni, C., Harabaglia, P., Merlini, S., Mongelli, F., Peccerillo, A., & Piromallo, C. (1999). Orogens and slabs vs. their direction of subduction. *Earth-Science Reviews*, *45*(3–4), 167–208. https://doi.org/10.1016/S0012-8252(98)00045-2

Doglioni, C., Innocenti, F., Morellato, C., Procacciani, D., & Scrocca, D. (2004). On the Tyrrhenian Sea opening. *Memorie Descrittive della Carta Geologica D'Italia*, *64*, 147–164.

Dunn, R. A., & Martinez, F. (2011). Contrasting crustal production and rapid mantle transitions beneath back-arc ridges. *Nature*, *469*(7329), 198–202. https://doi.org/10.1038/nature09690

Ellis, R. G., & MacLeod, I. N. (2013). Constrained voxel inversion using the Cartesian cut cell method. *ASEG Extended Abstracts*, *2013*(1), 1–4. https://doi.org/10.1071/ASEG2013ab222

EMODnet Bathymetry Consortium. (2020). EMODnet digital bathymetry (DTM 2020) [Dataset]. https://doi.org/10.12770/bb6a87dd-e579-4036-abe1-e649cea9881a

Faccenna, C., Becker, T. W., Lucente, F. P., Jolivet, L., & Rossetti, F. (2001). History of subduction and back-arc extension in the Central Mediterranean. *Geophysical Journal International*, *145*(3), 809–820. https://doi.org/10.1046/j.0956-540x.2001.01435.x

Faggioni, O., Pinna, E., Savelli, C., & Schreider, A. A. (1995). Geomagnetism and age study of Tyrrhenian seamounts. *Geophysical Journal International*, *123*(3), 915–930. https://doi.org/10.1111/j.1365-246X.1995.tb06898.x

Gallotti, G., Zaniboni, F., Arcangeli, D., Angeli, C., Armigliato, A., Cocchi, L., et al. (2023). The tsunamigenic potential of landslide-generated tsunamis on the Vavilov seamount. *Journal of Volcanology and Geothermal Research*, *434*, 107745. https://doi.org/10.1016/j.jvolgeores.2023.107745

Ha, G., Montési, L. G. J., & Zhu, W. (2023). Geometrical relations between slab dip and the location of volcanic arcs and back-arc spreading centers. *Geochemistry, Geophysics, Geosystems*, *24*(8), e2023GC010997. https://doi.org/10.1029/2023GC010997

Holt, A. F., & Royden, L. H. (2020). Subduction dynamics and mantle pressure: 2. Towards a global understanding of slab dip and upper mantle circulation. *Geochemistry, Geophysics, Geosystems*, *21*(7). https://doi.org/10.1029/2019GC008771

Hsu, K., Montadert, L., Bernoulli, D., Cita, M. B., Erickson, A., Garrison, R. E., et al. (1978). *Initial reports of the deep sea drilling project* (Vol. 42, Pt. 1). U.S. Government Printing Office. https://doi.org/10.2973/dsdp.proc.42-1.1978

Ingram, D. M., Causon, D. M., & Mingham, C. G. (2003). Developments in Cartesian cut cell methods. *Mathematics and Computers in Simulation*, *61*(3–6), 561–572. https://doi.org/10.1016/S0378-4754(02)00107-6

Karig, D. E. (1971). Origin and development of marginal basins in the western Pacific. *Journal of Geophysical Research*, *76*(11), 2542–2561. https://doi.org/10.1029/JB076i011p02542

Kastens, K. A., Mascle, J., Auroux, C., Bonatti, E., Broglia, C., Channell, J., et al. (Eds.). (1990). *Proceedings of the ocean drilling program, 107 scientific results* (Vol. 107). Ocean Drilling Program. https://doi.org/10.2973/odp.proc.sr.107.1990

Kastens, K. A., Mascle, J., Auroux, C., Bonatti, E., Broglia, C., Channell, J., et al. (1988). ODP Leg 107 in the Tyrrhenian Sea: Insights into passive margin and back-arc basin evolution. *Geological Society of America Bulletin*, *100*(7), 1140–1156. https://doi.org/10.1130/0016-7606(1988)100<1140:OLITTS>2.3.CO;2

Klügel, A., Longpré, M.-A., García-Cañada, L., & Stix, J. (2015). Deep intrusions, lateral magma transport and related uplift at ocean island volcanoes. *Earth and Planetary Science Letters*, *431*, 140–149. https://doi.org/10.1016/j.epsl.2015.09.031

Li, S., Suo, Y., Li, X., Liu, B., Dai, L., Wang, G., et al. (2018). Microplate tectonics: New insights from micro-blocks in the global oceans, continental margins and deep mantle. *Earth-Science Reviews*, *185*, 1029–1064. https://doi.org/10.1016/j.earscirev.2018.09.005

Loreto, M. F., Zitellini, N., Ranero, C. R., Palmiotto, C., & Prada, M. (2021). Extensional tectonics during the Tyrrhenian back-arc basin formation and a new morpho-tectonic map. *Basin Research*, *33*(1), 138–158. https://doi.org/10.1111/bre.12458

Magrini, F., Diaferia, G., El-Sharkawy, A., Cammarano, F., Van Der Meijde, M., Meier, T., & Boschi, L. (2022). Surface-wave tomography of the central-western Mediterranean: New insights into the Liguro-Provençal and Tyrrhenian basins. *Journal of Geophysical Research: Solid Earth*, *127*(3), e2021JB023267. https://doi.org/10.1029/2021JB023267

Malinverno, A., & Ryan, W. B. F. (1986). Extension in the Tyrrhenian Sea and shortening in the Apennines as result of arc migration driven by sinking of the lithosphere. *Tectonics*, *5*(2), 227–245. https://doi.org/10.1029/TC005i002p00227

Manu-Marfo, D., Aoudia, A., Pachhai, S., & Kherchouche, R. (2019). 3D shear wave velocity model of the crust and uppermost mantle beneath the Tyrrhenian basin and margins. *Scientific Reports*, *9*(1), 3609. https://doi.org/10.1038/s41598-019-40510-z

Mascle, J., & Rehault, J.-P. (1990). A revised seismic stratigraphy of the Tyrrhenian Sea: Implications for the basin evolution. *Proceedings of the Ocean Drilling Program, Scientific Results, ODP, Leg 107, Tyrrhenian Sea*, *107*, 617–636. https://doi.org/10.2973/odp.proc.sr.107.181.1990

Menand, T., Annen, C., & De Saint Blanquat, M. (2015). Rates of magma transfer in the crust: Insights into magma reservoir recharge and pluton growth. *Geology*, *43*(3), 199–202. https://doi.org/10.1130/G36224.1

Milia, A., Torrente, M. M., & Tesauro, M. (2017). From stretching to mantle exhumation in a triangular backarc basin (Vavilov basin, Tyrrhenian Sea, Western Mediterranean). *Tectonophysics*, *710–711*, 108–126. https://doi.org/10.1016/j.tecto.2016.10.017

Muccini, F., Cocchi, L., Locritani, M., & Carmisciano, C. (2016). Sea-surface and deep-magnetic data at Vavilov Seamount, Tyrrhenian Sea. In *Geophysical Research abstracts* (Vol. 18). EGU2016-6124. http://hdl.handle.net/2122/10404

Muller, J. R., Ito, G., & Martel, S. J. (2001). Effects of volcano loading on dike propagation in an elastic half-space. *Journal of Geophysical Research*, *106*(B6), 11101–11113. https://doi.org/10.1029/2000JB900461

Palmiotto, C., Braga, R., Corda, L., Di Bella, L., Ferrante, V., Loreto, M. F., & Muccini, F. (2022). New insights on the fossil arc of the Tyrrhenian Back-Arc basin (Mediterranean Sea). *Tectonophysics*, *845*, 229640. https://doi.org/10.1016/j.tecto.2022.229640

Palmiotto, C., Ficini, E., Loreto, M. F., Muccini, F., & Cuffaro, M. (2022). Back-Arc spreading centers and superfast subduction: The case of the northern Lau Basin (SW Pacific Ocean). *Geosciences*, *12*(2), 50. https://doi.org/10.3390/geosciences12020050

Pearce, J. A., & Stern, R. J. (2006). Origin of back-arc basin magmas: Trace element and isotope perspectives. In D. M. Christie, C. R. Fisher, S.-M. Lee, & S. Givens (Eds.), *Geophysical monograph series* (Vol. 166, pp. 63–86). American Geophysical Union. https://doi.org/10.1029/166GM06

Pinel, V., Carrara, A., Maccaferri, F., Rivalta, E., & Corbi, F. (2017). A two-step model for dynamical dike propagation in two dimensions: Application to the July 2001 Etna eruption: Dynamical Dike Propagation in 2D. *Journal of Geophysical Research: Solid Earth*, *122*(2), 1107–1125. https://doi.org/10.1002/2016JB013630

Polonia, A., Torelli, L., Gasperini, L., Cocchi, L., Muccini, F., Bonatti, E., et al. (2017). Lower plate serpentinite diapirism in the Calabrian Arc subduction complex. *Nature Communications*, *8*(1), 2172. https://doi.org/10.1038/s41467-017-02273-x

Prada, M., Ranero, C. R., Sallarès, V., Zitellini, N., & Grevemeyer, I. (2016). Mantle exhumation and sequence of magmatic events in the Magnaghi–Vavilov Basin (Central Tyrrhenian, Italy): New constraints from geological and geophysical observations. *Tectonophysics*, *689*, 133–142. https://doi.org/10.1016/j.tecto.2016.01.041

Robin, C., Colantoni, P., Gennesseaux, M., & Rehault, J. P. (1987). Vavilov seamount: A mildly alkaline Quaternary volcano in the Tyrrhenian basin. *Marine Geology*, *78*(1–2), 125–136. https://doi.org/10.1016/0025-3227(87)90071-5

Sartori, R., Torelli, L., Zitellini, N., Carrara, G., Magaldi, M., & Mussoni, P. (2004). Crustal features along a W–E Tyrrhenian transect from Sardinia to Campania margins (central Mediterranean). *Tectonophysics*, *383*(3–4), 171–192. https://doi.org/10.1016/j.tecto.2004.02.008

Savelli, C. (2002). Time–space distribution of magmatic activity in the western Mediterranean and peripheral orogens during the past 30 Ma (a stimulus to geodynamic considerations). *Journal of Geodynamics*, *34*(1), 99–126. https://doi.org/10.1016/S0264-3707(02)00026-1

Savelli, C., & Ligi, M. (2017). An updated reconstruction of basaltic crust emplacement in Tyrrhenian Sea, Italy. *Scientific Reports*, *7*(1), 18024. https://doi.org/10.1038/s41598-017-17625-2

Schellart, W. P., Jessell, M. W., & Lister, G. S. (2003). Asymmetric deformation in the backarc region of the Kuril arc, northwest Pacific: New insights from analogue modeling. *Tectonics*, *22*(5). https://doi.org/10.1029/2002TC00147

Schliffke, N., Van Hunen, J., Allen, M. B., Magni, V., & Gueydan, F. (2022). Episodic back-arc spreading centre jumps controlled by transform fault to overriding plate strength ratio. *Nature Communications*, *13*(1), 582. https://doi.org/10.1038/s41467-022-28228-5

Scrocca, D., Carminati, E., Doglioni, C., & Procaccianti, D. (2012). Tyrrhenian Sea. In *Regional geology and tectonics: Phanerozoic passive margins, cratonic basins and global tectonic maps* (pp. 472–485). Elsevier. https://doi.org/10.1016/B978-0-444-56357-6.00012-3

Sdrolias, M., & Müller, R. D. (2006). Controls on back-arc basin formation. *Geochemistry, Geophysics, Geosystems*, *7*(4), 2005GC001090. https://doi.org/10.1029/2005GC001090

Stern, R. J. (2002). Subduction zones. *Reviews of Geophysics*, *40*(4), 3-1–3-38. https://doi.org/10.1029/2001RG000108

Tibaldi, A. (2015). Structure of volcano plumbing systems: A review of multi-parametric effects. *Journal of Volcanology and Geothermal Research*, *298*, 85–135. https://doi.org/10.1016/j.jvolgeores.2015.03.023

Tibaldi, A., & Pasquarè, F. A. (2008). A new mode of inner volcano growth: The "flower intrusive structure". *Earth and Planetary Science Letters*, *271*(1–4), 202–208. https://doi.org/10.1016/j.epsl.2008.04.009

Ventura, G., Milano, G., Passaro, S., & Sprovieri, M. (2013). The Marsili Ridge (Southern Tyrrhenian Sea, Italy): An island-arc volcanic complex emplaced on a 'relict' back-arc basin. *Earth-Science Reviews*, *116*, 85–94. https://doi.org/10.1016/j.earscirev.2012.11.005

Wei, S. S., & Wiens, D. A. (2020). High bulk and shear attenuation due to partial melt in the Tonga-Lau back-arc mantle. *Journal of Geophysical Research: Solid Earth*, *125*(1). https://doi.org/10.1029/2019JB017527

Wessel, P., & Smith, W. H. F. (1998). New, improved version of generic mapping tools released. *Eos, Transactions American Geophysical Union*, *79*(47), 579. https://doi.org/10.1029/98EO00426